Recent developments of the HEPD-02 detector, on board the CSES-02 satellite

S. Amoroso(1)(2) *on behalf of the CSES-Limadou Collaboration*

(1) *INFN, Sezione di Roma Tor Vergata - Roma, Italy.*
(2) *University of Roma Tor Vergata, V. della Ricerca Scientifica 1, 00133 Roma, Italy*

Summary. — The Italo–Chinese CSES–LIMADOU mission, inaugurated on September 25, 2013, plans to deploy multiple satellites over the upcoming years. CSES-02 was successfully launched on June 14, 2025. Equipped with 11 payloads, the mission aims to study the interactions among Earth's lithosphere, atmosphere, ionosphere, and magnetosphere; extend measurements of low-energy cosmic rays across various particle species; analyze Sun–Earth interactions; monitor the Van Allen belts. One of the instruments onboard CSES-02 is HEPD-02 (High-Energy Particle Detector), a completely Italian-built upgrade of HEPD-01 previously launched on the first satellite of the mission, CSES-01. It comprises three planes of pixel trackers and an electromagnetic calorimeter made from plastic scintillators and LYSO crystals. HEPD-02 measures charged-particle fluxes, principally protons (30–200 MeV), electrons (3–100 MeV), and light nuclei, in low Earth orbit, achieving high energy and angular resolution. Its enhanced trigger logic enables precise flux monitoring in high-radiation regions like the South Atlantic Anomaly and detection of gamma-ray transients (Gamma-Ray Bursts). This article provides a detailed description of HEPD-02's sub-detectors, emphasizing improvements over its predecessor. It also discusses detector performance, based on ground tests with accelerator beams and cosmic-ray muons.

1. – CSES-Limadou collaboration

The CSES (China Seismo-Electromagnetic Satellite) [1]-Limadou mission is a scientific collaboration between the Italian Space Agency (ASI) and the China National Space Administration (CNSA), initiated on 25 September 2013. It encompasses the design, construction, and launch of multiple satellites dedicated to study Earth's geophysical characteristics.
The first satellite, CSES-01, was launched in February 2018 into a Sun-synchronous orbit at approximately 500 km altitude and continues to collect scientific data. Its successor, CSES-02, was successfully launched on 14 June 2025 into a similar orbit with 98° inclination and is expected to remain operational for about six years. Unlike CSES-01, which

halted data acquisition above $\pm 70^\circ$ latitude, CSES-02, thanks to upgraded instrumentation, enables continuous operation across all latitudes, including polar regions.
The primary scientific objective of the CSES mission is to investigate the coupling mechanisms among the lithosphere, atmosphere, ionosphere, and magnetosphere, and to determine how these interactions generate perturbations in the upper ionosphere and near the inner edge of the radiation belts. Additionally, the satellites carry instruments capable of measuring electromagnetic fields, plasma properties, and low energy charged particles. Mission goals include extending measurements of low-energy cosmic rays (protons, electrons, and light nuclei), analyzing Sun–Earth interactions, and monitoring the Van Allen radiation belts.

2. – Scientific goals of HEPD-02

One of the Italian contributions to the CSES-02 satellite is the Limadou HEPD-02 detector. HEPD-02 is designed to measure fluxes of protons (30–200 MeV), electrons (3–100 MeV), and light nuclei, and to investigate possible correlations between enhancements in these fluxes and short-term perturbations of the radiation belts caused by solar activity or events of terrestrial or anthropogenic origin [2].
To achieve this, the detector is capable of detecting individual incident particles, identifying their nature (protons, electrons, or light nuclei), measuring their energy, and determining the pitch angle, that is, the angle between the particle's trajectory and the direction of the local geomagnetic field line. In this context, HEPD-02 plays a key role in studying sudden increases in particle fluxes ("particle bursts") originating from disturbances in the Earth's magnetosphere, particularly those related to the loss of trapped particles from the inner Van Allen belt. By accurately reconstructing the energy spectrum and the spatial origin of these events, the detector aims to identify potential temporal correlations with terrestrial seismic phenomena [2].
Beyond these studies, HEPD-02 also contributes to the investigation of galactic cosmic rays and solar modulation effects [3]. The combination of data from HEPD-01, which operated during the solar minimum, and HEPD-02, which began data acquisition near the current solar maximum, is expected to cover most of a solar cycle. This will enable a comprehensive analysis of the long-term evolution of solar activity and its impact on the near-Earth radiation environment. Additional scientific objectives include the observation of solar energetic particles (SEPs) and, more broadly, the measurement of the fluxes of charged particles, both incoming from space and those trapped within the Earth's magnetosphere [4]. Furthermore, thanks to the implementation of dedicated trigger masks, HEPD-02 is equipped to detect transient astrophysical phenomena such as gamma-ray bursts (GRBs) [5-7].

3. – Structure of the HEPD-02 and main changes compared to the HEPD-01

The detector (fig. 1) consists of a first trigger plane (TR1) made of five scintillator bars (dimensions of each bar 154.6×32.5 mm^2, 2 mm thick) followed by a tracking layer (DIR) consisting of five towers (dimensions of each tower on the xy plane 150×30 mm^2) that uses monolithic active pixel sensors (MAPS) to reconstruct the trajectories of incoming particles. This is succeeded by a second trigger plane (TR2) consisting of 4 bars (dimensions of each bar 36×150 mm^2, 8 mm thick), and finally the calorimeter, which includes 12 thin layers (RAN) (dimensions of each layer 150×150 mm^2, 10 mm thick) and two thicker layers (EN) made of LYSO crystals, each divided into three bars (dimen-

sions of each bar 150 × 49 mm^2, 25 mm thick) where the incident particles deposit most of their energy [2]. The calorimeter readout uses plastic scintillators coupled to photomultiplier tubes (PMTs) [8]. Finally, the detector is surrounded by an anticoincidence system made by 5 plastic scintillator planes (VETO).

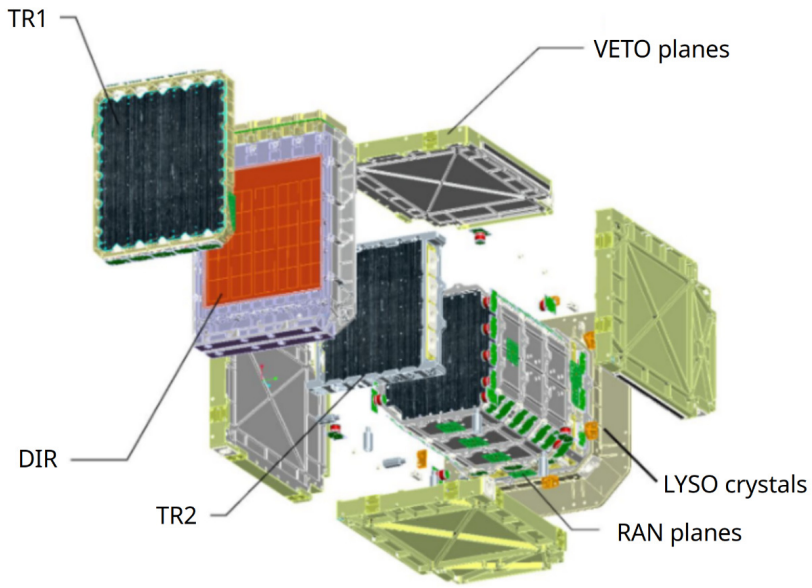

Fig. 1.: CAD image of HEPD-02 detector.

In table I HEPD-02 specifications are summarized

TABLE I.: Key operational specifications of HEPD-02.

Parameter	**Value**
Operating temperature	$-10\,^{\circ}$C to $35\,^{\circ}$C
Operating pressure	$\leq 6.65 \times 10^{-3}$ Pa
Data budget	≤ 100 Gb/day
Mass budget	≤ 50 kg
Power budget	≤ 45 W
Electron kinetic energy range	3 MeV to 100 MeV
Proton kinetic energy range	30 MeV to 200 MeV
Pointing	Zenith
Scientific data bus	RS-422
Data handling bus	CAN 2.0
Life cycle	> 6 years

Now we briefly outline the improvements implemented in HEPD-02. First of all, a MAPS tracker is used in space for the first time. It consists of three planes, each made of five independent bars with pixels featuring a 29.4 μm pitch along x and 26.88 μm pitch along y [8]. Unlike its predecessor, HEPD-02 includes two trigger planes. The first, TR1,

is composed of five bars with a thickness of 0.2 cm, while the second, TR2, consists of four bars with a thickness of 0.8 cm, oriented orthogonally to the first. This configuration allowed us to decrease the energy threshold and increase redundancy.
HEPD-02 has an upgraded trigger logic enabling it to acquire with concurrent and prescalable trigger masks. This feature improves data acquisition even in high-radiation regions such as the South Atlantic Anomaly (SAA) or polar areas.
The number of calorimeter planes has been reduced from 16 to 12. The final part of the calorimeter consists of two planes, each divided into three LYSO crystal bars arranged orthogonally to each other. Unlike HEPD-01, which used 9 cubes of LYSO crystals, HEPD-02 allows for the readout of individual bars using two photomultiplier tubes placed at the ends, thus enhancing redundancy.
Finally, as previously mentioned, HEPD-02 remains fully operational at all latitudes, collecting data even over the poles.

4. – HEPD-02 data analysis and calorimeter equalization

In this section, we describe the work carried out to equalize the calorimeter response and eliminate the dependence of the reconstructed deposited energy on the impact position of incoming particles. The analysis presented here is based on data acquired during the 2023–2024 test beam campaign. Specifically, we used 228 MeV protons acquired from the Protontherapy Center in Trento, as well as cosmic muon acquisition runs. The 228 MeV run was selected because, at this energy, protons reach the last layer of the calorimeter, enabling a full-depth characterization of the detector. Moreover, the beam configuration used during this run was optimized to uniformly illuminate the entire detector surface.
As a first step, using the tracking planes, we reconstructed the muon trajectories and propagated them through the calorimeter planes. Each plane was then virtually divided into cells, and for each cell we studied the energy deposited by events whose tracks intersected it. In particular, we performed a Landau fit on these distributions and extracted the Most Probable Value (MPV).

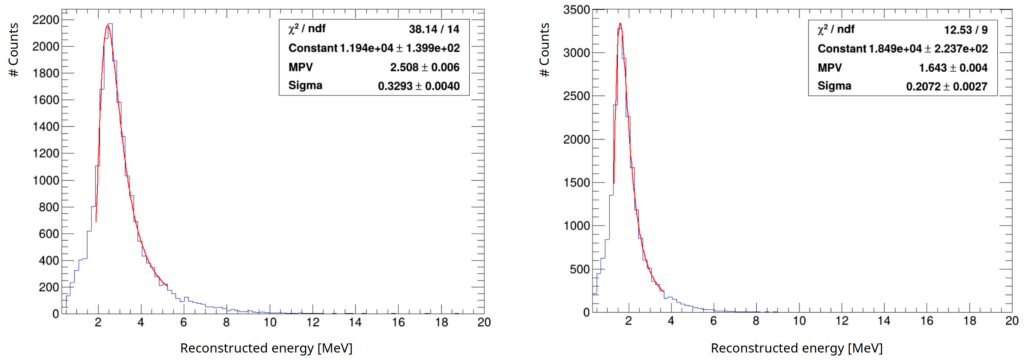

(a) Energy distribution of a single cell of the first RAN plane before the equalization.

(b) Energy distribution of a single cell of the first RAN plane after the equalization.

Fig. 2.: Landau fit of the reconstructed energy in an angular cell of the first RAN plane with single-PMT readout, where photon collection asymmetry is enhanced.

As an example, fig. 2 shows the Landau fit of the reconstructed energy distribution for a single cell in the first RAN plane, before equalization (fig. 2a) and after equalization (fig. 2b). Then we plotted each MPV obtained in a 2D map for each calorimeter plane. Figure 3a shows, as an example, the MPV map for the energy distributions of the first RAN plane.

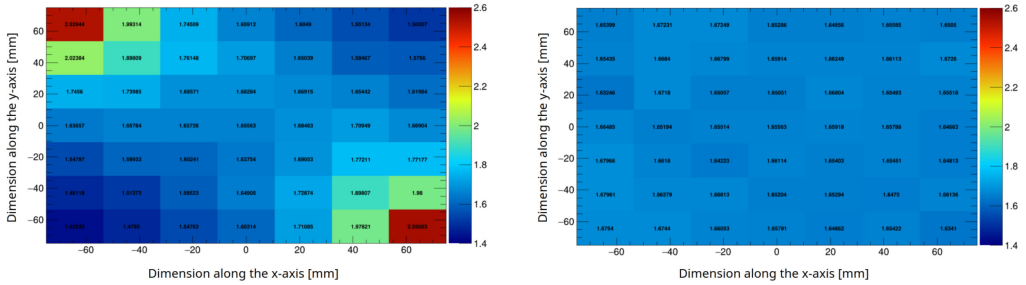

(a) MPV map of the first RAN plane before the equalization.

(b) MPV map of the first RAN plane after the equalization.

Fig. 3.: Cells maps of the first RAN plane. In each cell it is written the MPV (MeV) of the Landau distribution of the reconstructed energy for a cosmic muons acquisition runs.

This plot reveals two key features that were central to the calorimeter equalization process. First, we observed that the central cells exhibit minimal dependence of the reconstructed energy on the muon impact position. For this reason, we chose the MPV of the central cell in each plane as the reference normalization value for the entire plane. Furthermore, we noticed that in the corner cells where the PMTs are installed (*i.e.* top-left and bottom-right in fig. 3a), the reconstructed energy shows significantly higher MPVs, approximately twice the value of the central cell. Conversely, the cells located in the opposite diagonal corners (*i.e.* farthest from the PMTs) exhibit the lowest MPVs. This behavior can be interpreted by considering that, unlike the PMT-side cells, those on the opposite diagonal experience a higher photon dispersion rate, resulting in a lower collected signal.

We therefore decided to rescale the reconstructed energy in each individual cell using multiplicative correction factors, defined as the ratio between the MPV of that cell and the MPV of the central cell in the same calorimeter plane. As an example, fig. 3b shows the MPV map for the first RAN plane after applying the energy rescaling factors to each cell, leading to a more uniform distribution of values compared to the case without equalization.

We now briefly describe the final step carried out to obtain a quantitative estimate of the result achieved through the equalization process. For each calorimeter plane, we divided the MPV of each single cell by the MPV of the central cell, which was used as the reference value for normalization. For each calorimeter sector (*i.e.* TR1, TR2, RAN, EN1, EN2), we then built the distribution of these ratios in both the equalized and non-equalized cases. As an example, we report below the distribution of these ratios for the RAN planes (fig. 4). As can be seen, in the equalized case (fig. 4b) the distribution is significantly narrower around 1, indicating the improvement brought by the equalization process compared to the non-equalized case (fig. 4a).

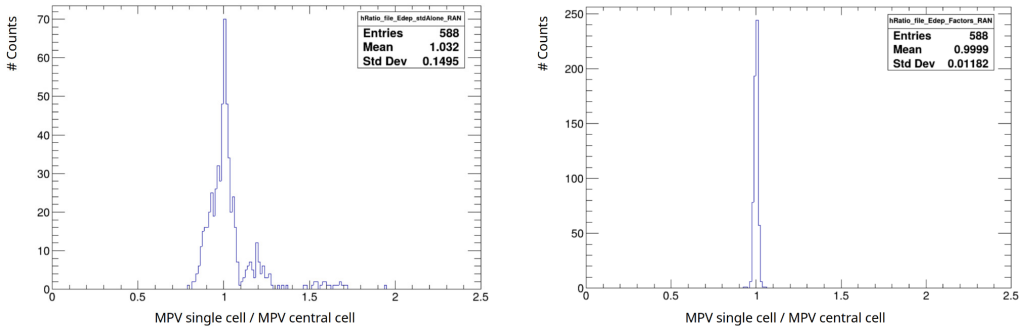

(a) Ratios before the equalization.

(b) Ratios after the equalization.

Fig. 4.: Distribution of the ratios between the MPV of each single cell with the central MPV of the first RAN plane.

5. – Conclusions

In this work, we have presented the High Energy Particle Detector HEPD-02, currently operating onboard the CSES-02 satellite, which has been in orbit since June 14. We outlined its main features and the improvements made compared to its predecessor, HEPD-01, launched aboard CSES-01 and in operation since February 2018.
We highlighted the scientific goals of the detector within the broader framework of the CSES mission.
Finally, based on data collected during the 2023–2024 test beam campaign and cosmic muon acquisition runs, we described the equalization procedure performed on the calorimeter planes. We showed how the applied corrections significantly improved the uniformity and accuracy of the instrument's response in reconstructing the energy deposited by incoming particles.

REFERENCES

[1] Shen, X. *et al.*, *Science China Technological Sciences*, **61** (2018) 634.
URL `https://doi.org/10.1007/s11431-018-9242-0`
[2] De Santis C. and Ricciarini S., *The High Energy Particle Detector (HEPD-02) for the second China Seismo-Electromagnetic Satellite (CSES-02)*, in proc. of *Proceedings of 37th International Cosmic Ray Conference — PoS(ICRC2021)*, Vol. 395 2021, p. 058.
[3] Martucci, M. *et al.*, *The Astrophysical Journal Letters*, **945** (2023) L39.
URL `https://dx.doi.org/10.3847/2041-8213/acbea7`
[4] Bartocci, S. *et al.*, *Journal of Instrumentation*, **20** (2025) P06005.
URL `https://dx.doi.org/10.1088/1748-0221/20/06/P06005`
[5] Palma, F. *et al.*, *The Astrophysical Journal*, **960** (2023) 21.
URL `https://dx.doi.org/10.3847/1538-4357/ad06ae`
[6] Battiston, R. *et al.*, *The Astrophysical Journal Letters*, **946** (2023) L29.
URL `https://dx.doi.org/10.3847/2041-8213/acc247`
[7] Bartocci, S. *et al.*, *The Astrophysical Journal*, **976** (2024) 239.
URL `https://dx.doi.org/10.3847/1538-4357/ad822c`
[8] Bartocci S. *et al.*, *Nuclear Instruments and Methods in Physics Research Section A: Accelerators, Spectrometers, Detectors and Associated Equipment*, **1080** (2025) 170756.
URL `https://www.sciencedirect.com/science/article/pii/S0168900225005571`